Deep-Blue Light-Emitting Polyfluorenes with Asymmetrical Naphthylthio-Fluorene as Chromophores

Liwen Hu,[1,2] Zhonglian Wu,[3] Xiaojun Wang,[1] Yawei Ma,[1] Ting Guo,[1] Lei Ying,[1,2] Junbiao Peng,[1] Yong Cao[1]

[1]Institute of Polymer Optoelectronic Materials and Devices, State Key Laboratory of Luminescent Materials and Devices, South China University of Technology, Guangzhou 510640, China
[2]South China Institute of Collaborative Innovation, Dongguan 523808, China
[3]School of Materials Engineering, Jiangsu University of Technology, Changzhou 213001, China
Correspondence to: T. Guo (E-mail: mstguo@scut.edu.cn) or L. Ying (E-mail: msleiying@scut.edu.cn)

Received 25 September 2018; accepted 7 November 2018
DOI: 10.1002/pola.29283

ABSTRACT: A novel blue polycyclic aromatic compound 2,8-dibromo-14,14-dioctyl-14*H*-benzo[*b*]benzo [5,6] fluoreno[1,2-*d*] thiophene 9,9-dioxide (Br_2NFSO) is designed and synthesized through multistep synthesis, and its structure is confirmed by nuclear magnetic resonance. Based on synthesized polycyclic aromatic compound Br_2NFSO, a series of twisted blue light-emitting polyfluorenes derivatives (PNFSOs) are prepared by one-pot Suzuki polycondensation. Based on the twisted polymer molecular structure resulted from the asymmetric links of 14,14-dioctyl-14H-benzo[b]benzo[5,6]fluoreno [1,2-d]thiophene 9,9-dioxide (NFSO) unit in copolymers and better electron transport ability of NFSO than those of the electron-deficient dibenzothiophene-*S,S*-dioxide counterpart, the resulting polymers exhibit excellent electroluminescent spectra stability in the current densities from 100 to 800 mA cm^{-2}, and show blue-shifted and narrowed electroluminescent spectra with the Commission Internationale de L'Eclairage (CIE) of (0.16, 0.07) for PNFSO5, compared to poly(9,9-dioctylfluorene) (PFO) with the CIE of (0.18, 0.18). Moreover, the superior device performance is achieved based on PNFSO5 with the maximum luminous efficiency (LE_{max}) of 1.96 cd A^{-1}, compared with the LE_{max} of 0.49 cd A^{-1} for PFO. The results indicate that the twisted polycyclic aromatic structure design strategy has a great potential to tuning blue emission spectrum and improving EL efficiency of blue light-emitting polyfluorenes. © 2018 Wiley Periodicals, Inc. J. Polym. Sci., Part A: Polym. Chem. **2018**

KEYWORDS: intromolecular charge transfer; polymer light-emitting diodes; polycyclic aromatic compound; synthesis; twisted structure

INTRODUCTION Depended on flexible display, solid-state lighting, low energy consumption, and low driving voltage, polymer light-emitting diodes have attracted great attention in the past decades.[1–5] Among three primary color polymers used in full-color flat panel displays, the red and green light-emitting polymers had already developed maturely. On the contrary, the blue-light emitting polymers still could not meet practical display applications, for example, the color purity, luminous efficiency, and spectra stability,[6,7] owing to the inherent wide band-gap nature. As reported, only a limited number of blue polymers exhibited excellent performance. As one of the promising blue emitters, polyfluorenes (PFs) are attractive because of its high photoluminescence quantum efficiency (PLQY), good thermal and electrochemical stability and facile functionalization at the C-9 position of the fluorene unit.[8,9] However, due to fluorenone defect formation and the poor electron transport ability,[10–12] the color purity of PFs is unsatisfactory, and the efficiency of the devices based on such emitters are still low, which limited its extensive application.

To improve color purity of PFs, much effort has been done. For example, 3,6-linkages fluorene or spirobifluorene were adopted as a building block to design deep blue-emitting PFs. Compared with 27-PFs, poly(9,9-dialkylfluorene-3,6-diyl) (36-PFs) showed a significantly blue-shifted electroluminescence (EL) spectra with maximum emission wavelength at about 415 nm and stable EL emission resulted from shorter conjugation length and twisted structure design.[13–15] The chemical stability of PFs was improved remarkably benefiting

Additional supporting information may be found in the online version of this article.

L. W. Hu and Z. L. Wu contributed equally to this work.

from the spiro-linkage at the 9-position of fluorene, which increased a large steric hindrance of fluorene unit warping in polymer backbone and restrained the appearance of fluorenone defect. What is more, this large steric hindrance of the vertical configuration of spirobifluorene can suppress their aggregation in the solid state.[16–18] Unfortunately, they still suffer from poor device efficiency compared with PFs due to the unbalanced charge carrier transportation.

PF was famous *p*-type organic semiconductor polymer, so that it exhibited poor electron transport ability and unbalanced charge carrier injection and transportation.[18] To enhance its electron transport ability, much electron-withdrawing groups, such as sulfonyl, cyano, oxadiazole, and triazole, were introduced into polymer backbones or side chains, respectively. These results demonstrated that the incorporation of these electron-deficient units into PFs could enhance the electron injection and balance the charge carrier transportation, and further improve the device performances.[19–22] However, the charge transfer (CT) effect from such electron-rich units to electron-withdrawing groups was inevitably appeared, which result in the color impurity for blue emission. For example, poly[(fluorene)-*co*-dibenzothiophene-*S,S*-dioxide] (PFSO) was one of the most efficient blue light-emitting polymers ever reported. Whereas the electron-deficient dibenzo-thiophene-*S,S*-dioxide (SO) unit brought about the photoluminescent (PL) and electroluminescent spectra bathochromic shift inevitably caused by CT effect.[23,24] Subsequently, our team designed a series of PFs linked SO unit in alkyl side chain to keep a certain distance between the fluorene donor in main chain and SO acceptor in side chain. A blue-shift together with narrowing EL spectra was obtained compared with that of polymers containing SO unit in main chain, which was attributed to both improved electron injection/transportation and weak CT effect.[25] Nevertheless, the low luminous efficiency of 1.17 cd A^{-1} with CIE coordinates of (0.18, 0.11) was achieved, which may be due to the long distance between electron-deficient SO unit in side chain and polymer main chain.

In this manuscript, a novel polycyclic aromatic compound 2,8-dibromo-14,14-dioctyl-14*H*-benzo[*b*]benzo[5,6]fluoreno [1,2-*d*]thiophene 9,9-dioxide (Br$_2$NFSO) was designed and synthesized based on following consideration, (a) polycyclic aromatic compound had higher fluorescence quantum efficiency,[24] therefore the benzene moiety of fluorene unit was replaced by naphthalene moiety, (b) electron-deficient SO unit was rearranged into polycyclic aromatic compound because of better electron transport ability of SO unit, and SO unit can also increase the molecular weight of resulting monomer, (c) asymmetric molecular structure can disturb the effective conjugated length and improve the blue emission purity. A series of PF derivatives containing the NFSO unit were also prepared and studied in detail. The resulting copolymers exhibited weak CT effect, balanced charge carrier injection/transportation, superior EL efficiency and deep blue emission with respect to PFO, which can be attributed to indirect conjugation of SO moiety and the twisted polycyclic aromatic structure in copolymer backbone.[26]

EXPERIMENTAL

Materials

Commercially available reagents were used without further purification, unless stated otherwise. Toluene was purified by routine procedures and distilled in dry argon atmosphere before used.

Synthesis

2-Bromodibenzo[*b,d*]thiophene **(1)**, 2-(dibenzo [*b,d*]thiophen-2-yl)-4,4,5,5-tetramethyl-1,3,2-dioxaborolane **(2)**, methyl 1-bromo-2-naphthoate **(3)**, 2,7-bis(4,4,5,5-tetramethyl-1,3,2 -dioxaborolan-2-yl)-9,9-dioctylfluorene **(M2)**, 2,7-dibromo-9,9-dioctylfluorene **(M3)** were synthesized according to previous literatures.[27–30]

*Methyl 1-(Dibenzo[*b,d*]Thiophen-2-yl)-2-Naphthoate (4)*

In a 250 mL two-necked flask, Pd(PPh$_3$)$_4$ (1.82 g, 1.57 mmol) was added to a mixture of compound (3) (10.00 g, 37.72 mmol), compound (2) (9.75 g, 31.43 mmol), 50 wt% Na$_2$CO$_3$ aqueous solution (16.66 g/17.0 mL deionized water, 157.17 mmol), tetrabutyl-ammonium bromide (4.0 mg, 12.4 μmol), 100 mL toluene under N$_2$ atmosphere and reacted at 90 °C for 12 h. The cooled solution was extracted with toluene, and the organic layer was washed with brine. The crude product was purified by column chromatography on silica gel with dichloromethane/petroleum ether (1:5). Yield: 80%. ^{1}H NMR (500 MHz, CDCl$_3$) δ (ppm): 8.10 (d, *J* = 7.10 Hz, 2H), 7.99 (d, *J* = 5.95 Hz, 2H), 7.96–7.93 (m, 2H), 7.90 (d, *J* = 7.20 Hz, 1H), 7.61 (d, *J* = 8.60 Hz, 1H), 7.57 (t, *J* = 7.48 Hz, 1H), 7.48 (t, *J* = 7.50 Hz, 1H), 7.45–7.39 (m, 3H), 3.59 (s, 3H). ^{13}C NMR (125 MHz, CDCl$_3$) δ (ppm): 168.65, 141.25, 139.89, 138.51, 135.49, 138.51, 135.49, 135.37, 135.32, 134.80, 132.91, 128.52, 128.29, 127.94, 127.86, 127.55, 126.81, 126.73, 125.49, 124.39, 122.87, 122.51, 122.22, 121.77, 52.03. MS (APCI): *m/z* (%): 368.1 [M$^+$].

*9-(1-(Dibenzo[*b,d*]Thiophen-2-yl)Naphthalen-2-yl) Heptadecan-9-ol (5)*

In a 500 mL two-necked flask, compound (4) (10.0 g, 27.1 mmol) was dissolved in 300 mL dry THF and octylmagnesium bromide (C$_8$H$_{17}$MgBr) in THF(59.0 g, 271.4 mmol) was added slowly. The reaction was stirred and refluxed for 16 h, then it was quenched by deionized water and extracted by ethyl acetate. After removing the organic phase under reduced pressure, the crude product was used for the next step directly.

14,14-Dioctyl-14H-Benzo[b]Benzo[5,6]Fluoreno [1,2-d] Thiophene (6)

After compound (5) was dissolved in 150 mL dichloromethane completely, 1.0 mL BF$_3$ etherate was injected into the reaction solution with stirring for 4 h. Then it was quenched by deionized water and extracted by dichloromethane. The organic phase was removing under reduced pressure and the crude product was purified by column chromatography on silica gel with petroleum ether. Yield: 35%. ^{1}H NMR (500 MHz, CDCl$_3$) δ (ppm): 8.76 (d, *J* = 8.50 Hz, 1H), 8.59 (d, *J* = 8.45 Hz, 1H), 8.41 (d, *J* = 8.15 Hz, 1H), 8.01 (d, *J* = 7.60 Hz, 2H), 7.97 (t, *J* = 8.05 Hz, 2H), 7.77–7.72 (m, 2H), 7.62–7.59 (m, 3H), 2.75 (t, *J* = 7.55 Hz, 3H). ^{13}C NMR (125 MHz, $CDCl_3$) δ (ppm): 152.36, 150.26, 140.48, 139.54, 138.00, 133.71, 132.83, 129.53, 129.42, 129.04, 128.57, 128.48, 127.13, 126.82, 126.71, 126.36, 126.00, 125.15, 124.96, 124.36, 123.68, 121.92, 116.73, 56.14, 35.37, 30.93, 30.59, 28.71, 28.56, 28.36, 28.31, 27.96, 27.80, 26.21, 24.62, 22.71, 21.65, 21.42, 13.11, 12.95. MS (APCI): *m*/*z* (%): 547.4 [M$^+$].

2,8-Dibromo-14,14-Dioctyl-14H-Benzo[b]Benzo[5,6] Fluoreno[1,2-d]Thiophene (7)

Compound (6) (1.00 g, 1.83 mmoL) and two piece of I_2 were dissolved in 50 mL $CHCl_3$, a mixture Br_2 (642.91 mg, 4.02 mmol) in $CHCl_3$ was added slowly. It was stirred for 24 h in the dark and quenched by sodium bisulfite aqueous solution. The crude product was purified by column chromatography with petroleum ether. Yield: 70%. ^{1}H NMR (500 MHz, $CDCl_3$) δ (ppm): 8.60 (d, *J* = 8.45 Hz, 1H), 8.54 (s, 1H), 8.40 (d, *J* = 8.45 Hz, 1H), 8.30 (d, *J* = 8.15 Hz, 1H), 7.91 (d, *J* = 7.65 Hz, 1H), 7.82 (s, 1H), 7.75 (t, *J* = 8.05 Hz, 1H), 7.70 (t, *J* = 7.50 Hz, 1H), 7.65 (t, *J* = 7.48 Hz, 1H), 7.57 (t, *J* = 7.50 Hz, 1H), 2.68–2.62 (m, 2H), 2.12–2.06 (m, 2H), 1.08–0.84 (m, 24H), 0.47–0.31 (m, 6H). ^{13}C NMR (125 MHz, $CDCl_3$) δ (ppm): 151.99, 149.20, 144.84, 137.59, 133.20, 132.64, 130.78, 130.65, 129.92, 129.40, 128.90, 128.68, 128.11, 127.79, 127.05, 126.18, 125.92, 125.54, 123.57, 122.47, 121.87, 116.40, 56.20, 35.39, 30.92, 30.62, 28.69, 28.56, 28.34, 28.30, 27.97, 27.82, 26.19, 24.58, 22.74, 21.66, 21.41, 13.11, 12.98. MS (APCI): *m*/*z* (%):705.2 [M$^+$].

2,8-Dibromo-14,14-Dioctyl-14H-Benzo[b]Benzo[5,6] Fluoreno[1,2-d]Thiophene 9,9-Dioxide (M1)

Compound (7) (1.00 g, 1.42 mmol) was dissolved in 20 mL acetic acid, then 3.0 mL hydrogen peroxide was added and refluxed for 2 h. The reaction was quenched by deionized water and extracted by methylene dichloride. The product was purified by column chromatography on silica gel with dichloromethane/petroleum ether (1:1) and recrystallized with THF/Methanol. Yield: 50%. ^{1}H NMR (500 MHz, $CDCl_3$) δ (ppm): 8.68 (d, *J* = 8.45 Hz, 1H), 8.60 (s, 1H), 8.47 (d, *J* = 8.45 Hz, 1H), 8.37 (d, *J* = 8.15 Hz, 1H), 7.98 (d, *J* = 7.60 Hz, 1H), 7.90 (s, 1H), 7.82 (t, *J* = 7.65 Hz, 1H), 7.76 (t, *J* = 8.38 Hz, 1H), 7.72 (t, *J* = 8.10 Hz, 1H), 7.64 (t, *J* = 7.48 Hz, 1H), 2.75–2.69 (m, 2H), 2.19–2.12 (m, 2H), 1.13–0.89 (m, 24H), 0.55–0.41 (m, 6H). ^{13}C NMR (125 MHz, $CDCl_3$) δ (ppm): 152.99, 150.19, 145.84, 138.59, 134.21, 133.64, 131.77, 131.64, 130.93 130.40, 129.89, 129.68, 129.11, 128.78, 128.05, 127.17, 126.93, 126.54, 124.57, 123.47, 122.87, 111.39, 57.18, 36.36, 31.60, 29.56, 29.48, 28.97, 28.82, 23.73, 23.69, 22.44, 13.98. MS (APCI): *m*/*z* (%): 736.2 [M$^+$].

General Procedures for Suzuki Polycondensation, Taking PNFSO10 as an Examples

2,2′-(9,9-dioctyl-9*H*-fluorene-2,7-diyl) bis(4,4,5,5-tetramethyl-1,3,2-dioxa-borolane) (M2) (200 mg, 0.311 mmol), 2,7-dibromo-9,9-dioctyl-9*H*-fluorene (M3) (136.56 mg, 0.249 mmol), 2,8-dibromo-14,14-dioctyl-14*H*-benzo [*b*]benzo[5,6] fluoreno[1,2-*d*] thiophene 9,9-dioxide (M1) (45.86 mg, 0.062 mmol), palladium acetate ($Pd(OAc)_2$) (2.8 mg, 0.0125 mmol), and tricyclohexyl-phosphine (PCy_3) (6.98 mg, 0.249 mmol) were dissolved in 8 mL toluene under argon atmosphere, until the reaction was stirred clearly, tetraethyl ammonium hydroxide (Et_4NOH) (20% aq, 1.5 mL) was added and stirred at 80 °C for 24 h. The reaction was end-capped by phenylboronic acid (0.05 g, 0.4 mmol) for 12 h stirring. Finally, bromobenzene (0.125 g, 0.8 mmol) was added followed by stirring for another 12 h. After the reaction was cooled to room temperature, the mixture was precipitated with methanol and filtered. The crude product was further purified by Soxhlet extraction by methanol, acetone, and THF. The tetrahydrofuran component was repurified by column chromatography, and concentrated under reduced pressure, followed by reprecipitation methanol, drying under vacuum. Yield: 70%. ^{1}H NMR (500 MHz, $CDCl_3$) δ (ppm): 7.73–7.83 (br, ArH), 7.71–7.67 (br, ArH), 2.13 (br, CH_2), 1.22–1.14 (br, CH_2), 0.85–0.77 (br, CH_3). ^{13}C NMR (125 MHz, $CDCl_3$) δ (ppm): 151.84, 140.52, 126.19, 121.52, 120.00, 64.47, 55.35, 40.37, 31.80, 30.05, 29.23, 25.37, 22.61, and 14.08.

PNFSO2

M2 (200 mg, 0.311 mmol), **M3** (163.87 mg, 0.299 mmol), and **M1** (8.84 mg, 0.012 mmol). Yield: 71%. ^{1}H NMR (500 MHz, $CDCl_3$) δ (ppm): 7.85–7.80 (br, ArH), 7.71–7.63 (br, ArH), 2.12 (br, CH_2), 1.24–1.14 (br, CH_2), 0.83–0.80 (br, CH_3). ^{13}C NMR (125 MHz, $CDCl_3$) δ (ppm): 151.80, 140.48, 140.01, 126.14, 121.47, 119.95, 55.33, 40.37, 31.78, 30.30, 30.03, 29.21, 23.90, 22.59, and 14.05.

PNFSO5

M2 (200 mg, 0.311 mmol), **M3** (153.63 mg, 0.280 mmol), and **M1** (22.93 mg, 0.031 mmol). Yield: 73%. ^{1}H NMR (500 MHz, $CDCl_3$) δ (ppm): 7.85–7.80 (br, ArH), 7.71–7.67 (br, ArH), 2.13 (br, CH_2), 1.23–1.14 (br, CH_2), 0.84–0.70 (br, CH_3). ^{13}C NMR (125 MHz, $CDCl_3$) δ (ppm): 151.82, 140.52, 140.04, 126.17, 121.51, 119.98, 55.35, 40.39, 31.80, 30.05, 29.30, 29.23, 25.37, 23.92, 22.61, and 14.07.

PFO

M2 (200 mg, 0.311 mmol) and **M3** (200 mg, 0.311 mmol). Yield: 75%. ^{1}H NMR (500 MHz, $CDCl_3$) δ (ppm): 7.85–7.83 (br, ArH), 7.70–7.67 (br, ArH), 2.13 (br, CH_2), 1.22–1.14 (br, CH_2), 0.83–0.80 (br, CH_3). ^{13}C NMR (125 MHz, $CDCl_3$) δ (ppm): 151.84, 140.52, 140.03, 126.18, 121.51, 119.98, 55.35, 40.38, 31.80, 30.04, 29.23, 23.92, 22.61, and 14.07.

Instrumentation

Nuclear magnetic resonance (NMR) spectra were performed on Bruker Avance 500 spectrometer (operating at 500 MHz for ^{1}H NMR and 125 MHz for ^{13}C NMR), using deuterated chloroform as solution and the tetramethylsilane as the reference. The molecular weight and polydispersity index (PDI) were measured by gel permeation chromatography (GPC) using Waters Associates 515 GPC with polystyrene as standard and THF as eluent at room temperature, the concentration of the polymer sample is 2×10^{-3} g mL^{-1}. Thermogravimetric analysis (TGA) was recorded on a Netzsch

TG 209 at a heating rate of 20 °C min^{-1} with nitrogen flow. The differential scan calorimetry (DSC) was carried out by a Netzsch DSC 204 under N_2 atmosphere at a heating rate of 10 °C min^{-1}. UV–vis absorption spectra were recorded with a UV–vis–NIR light source (DT-MINI-2-GS, Ocean Optics) equipped with a QE65 Pro detector (Ocean Optics). Photoluminescence (PL) spectra were performed on a Spex Fluorolog-3 spectrofluorometer. Cyclic voltammetry (CV) were tested out by a CHI630E electrochemical work station, equipped with a glassy carbon working electrode, a saturated calomel electrode as the reference electrode, and a Pt wire counter electrode. The electrolyte solution was used as anhydrous acetonitrile tetrabutylammonium hexafluorophosphate in acetonitrile (0.1 M) under N_2 atmosphere. The density functional theory (DFT) calculation results were obtained by using Gaussian at the B3LYP/6-31G(d) level. Fluorescence quantum yields were measured using a Hamamatsu absolute PL quantum yield spectrometer C11347 Quantaurus-QY. The current density(J)-voltage (V)-luminance(L) characteristics of polymers were measured on a Keithley 236 source measurement unit. The luminance was calibrated by using a PR-705 Spectra Scan Spectro-photometer (Photo Research), with simultaneous acquisition of the EL spectra and CIE coordinates, driven by a Keithley model 2400 voltage–current source. Atomic force microscopy (AFM) measurements were performed on a Bruker Multimode 8 microscope in Scan Asyst in air mode. The films for AFM measurement were spin-coated on the top of the ITO/PEDOT:PSS surface.

Device Fabrication and Characterization

The structure of device was ITO/PEDOT:PSS/EML/Ba/Al. The sheet resistance of ITO glass substrates was 15–20 Ω/square. PEDOT:PSS layer with 40 nm was spin-coated on the top of the ITO glass substrate, which was treated by oxygen plasma, and the PEDOT:PSS film was heated at 180 °C for 10 min. Then the emission material PNFSOs were dissolved in *p*-xylene and the solution with concentration of 1.5×10^{-2} g mL^{-1} was deposited with a thickness of 60 nm. Finally, the device was finished after an 4 nm thick interface of Ba and an 200 nm thick cathode of Al. Excepted the deposition of PEDOT:PSS layer, all of the other procedures were carried out in the nitrogen filled glovebox. The thickness of each layer was measured by the thickness monitored using a Tencor Alpha-step 500 Surface Profilometer. The multilayer cathode was thermally deposited in a vacuum coating unit at base pressures $<10^{-5}$ mbar.

The hole-/electron-only devices were fabricated as ITO/PEDOT:PSS (40 nm)/polymer (80 nm)/MoO_3 (10 nm)/Al and ITO/ZnO (40 nm)/polymer (80 nm)/Ba (1.5 nm)/Al, respectively. To fabricate the hole-only device, a layer of MoO_3 (10 nm) instead of cesium fluoride was thermally deposited on top of the emission layer with a protective aluminum layer, with the remaining steps the same as those for the bipolar device. For the electron-only device, ITO glass was deposited with a layer of zinc oxide (40 nm) to replace the PEDOT:PSS film, then a thick copolymer layer (80 nm) was spin-cast from *p*-xylene solution on top of the zinc oxide layer and annealed at 100 °C for 20 min. Profilometry (Tencor Alfa-Step 500) was used to determine the thickness of the films. Finally, 1.5 nm of Ba followed by 100 nm of aluminum (thickness monitored with a STM-100/MF Sycon quartz crystal) were thermally evaporated through a shadow mask at a base pressure of 3.0×10^{-4} Pa to form the cathode.

RESULTS AND DISCUSSION

Synthesis of Monomers and Polymers

The synthetic route toward the monomers and the target polymers were outlined in Scheme 1. 2-(dibenzo[*b,d*]thiophen-2-yl)-4,4,5,5-tetra-methyl-1,3,2-dioxaborolane (2) was synthesized with 2-bromodibenzo[*b,d*] thiophene and 2-isopropoxy-4,4,5,5-tetramethyl-1,3,2-dioxaborolane as starting materials at −78 °C. Methyl 1-bromo-2-naphthoate (3) was obtained via esterification reaction in a good yield of 89%. Then methyl 1-(dibenzo[*b,d*]thiophen-2-yl)-2-naphthoate (4) was prepared by palladium-catalyzed Suzuki coupling reaction with a yield of 60%. Addition of the excess Grignard reagent *n*-octyl magnesium bromide to compound (4) produced the 9-(1-(dibenzo [*b,d*]thiophen-2-yl) naphthalene-2-yl) heptadecan-9-ol (5), and then it was ring-closed to generate 14,14-dioctyl-14*H*-benzo[*b*]benzo[5,6]fluoreno[1,2-*d*] thiophene 9,9-dioxide (6). The bromination of monomer 6 with bromine in chloroform gave the 2,8-dibromo-14,14-dioctyl-14*H*-benzo[*b*]benzo[5,6]fluoreno [1,2-*d*]thiophene 9,9-dioxide (7) in high yields. Finally, resulting monomer 2,8-dibromo-14,14-dioctyl-14*H*-benzo[*b*]benzo[5,6]fluoreno[1,2-*d*]thiophene 9,9-dioxide (M1) was synthesized through oxidizing reaction with hydrogen peroxide as oxidizer. The accurate assignment of aromatic protons of monomer M1 relied on the ^{1}H–^{1}H homonuclear correlation (COSY) experiments and ^{1}H-^{13}C heteronuclear multiple bond correlation of NMR spectroscopy with corresponding spectra shown in Figure 1(c,d). On the basis of peak split and the six group ^{1}H-^{1}H correlation signal in NMR spectrum [Fig. 1(b,c)], and correlation signal between singlet of δ = 7.90 ppm and quaternary carbon of δ = 57.2 ppm, and between singlet of δ = 8.61 ppm and quaternary carbon of δ = 117.4 ppm, δ = 134.24 ppm, and δ = 150.2 ppm [Fig. 1(d)], the exact bromination position of resulting monomer M1 can be confirmed and the result is our designed structure. The ^{13}C NMR and ^{1}H-^{13}C heteronuclear singular quantum correlation spectra were summarized in Supporting Information Figure S1.

The target polymers were synthesized through a palladium-catalyzed Suzuki polymerization, which were carried out by the molar feed ratios of M2:M3:M1 = 50:50:0, 50:48:2, 50:45:5, and 50:40:10, with relevant polymers denoted as PFO, PNFSO2, PNFSO5, and PNFSO10, respectively. The contrast polymers PFSO5 containing 5% dibenzothiophene-*S,S*-dioxide (SO) unit in polymer main chain and PF-FSO5 linked 5% SO moiety by long alkyl chain in polymer side chain were also prepared (Supporting Information Scheme S1). All polymers were easily dissolved in common organic solvents, such as tetrahydrofuran, chlorobenze, chloroform, and dichloromethane at room temperature, and showed superb film-

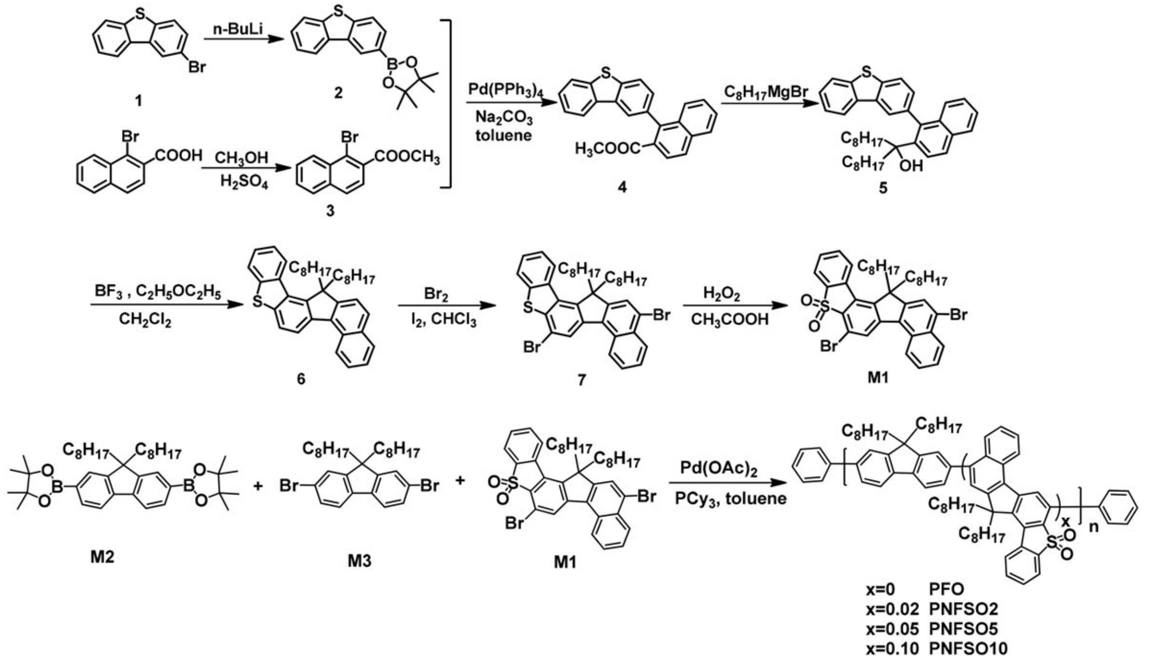

SCHEME 1 Synthetic routes for monomers and polymers.

forming ability by solution spin-coating processing. The number average molecular weight (M_n) of polymers was from 25.8 to 42.8 kDa, with the PDI in the range of 1.91–2.34. Detailed molecular weight data were summarized in Table 1.

Thermal Properties

DSC and TGA characteristics were conducted to assess the thermal properties of the resulting polymers as shown in the Figure 2 and Table 1. The copolymers presented the melting temperature (T_{m}) over 130 °C and the decomposition temperature (T_{d}) (corresponding to 5 wt % weight loss) over 420 °C, indicating the good thermal stability of polymers. This is important and desirable for optoelectronic applications. The T_{d}s of all copolymers are slightly lower than that of homopolymers PFO, indicating that the incorporation of NFSO unit into PFO increased the irregularities of polymer backbone attributed to the twisted-structure of monomer M1.[26] In addition, it can be seen that the T_{m} of copolymers increased gently as the fraction of NFSO unit increases, due to fused large polycyclic aromatic of NFSO unit. There was no obvious glass transition temperature during the heating process.

Electrochemical Properties

The electrochemical properties of the polymers were examined by CV. The reversible *p*-doping and *n*-doping traces of polymers were shown in Figure 3 and the detailed CV data were summarized in Table 1. With respect to all polymers, the oxidation potentials (E_{OX}) referred to ferrocene/ferrocenium (F_C/F_C+) was measured to be 0.39 V. It was assumed that the redox potential of F_c/F_c^+ was 4.80 eV relative to the vacuum energy level,[31,32] therefore, the highest occupied molecular orbital (HOMO) and the lowest unoccupied molecular orbital (LUMO) energy levels of the polymers were calculated according to the equations of $E_{\mathrm{HOMO}} = -(E_{\mathrm{ox}} + 4.80–0.39)$ eV and $E_{\mathrm{LUMO}} = -(E_{\mathrm{red}} + 4.80–0.39)$ eV. Thus, the E_{HOMOS} and E_{LUMOS} of polymers were estimated to be in the range of −5.75 eV to −5.77 eV and −2.26 to −2.16 eV, respectively. The EHOMO have no obvious change and the E_{LUMO} gently decreased with the increase of NFSO unit content in polymer, indicating the better electron transport ability of resulting polymers.

Photophysical Properties

Figure 4 displayed the UV–vis absorption and PL spectra in toluene solution and as thin film. In toluene, the absorption profiles of all polymers exhibited a strong absorption peaked at about 380 nm, which ascribed to the π-π^* transition of the conjugated backbone.[33] The absorption spectra for the films concisely correspond to those in solution, other than minor red-shifts and broadening of peaks. But for the PL spectra in toluene, all polymers showed a well-structured PL emission. And with the increase of NFSO unit, the PL intensity peaked at 416 nm kept unaltered, and that of the shoulder peaked around 436 nm remarkably enhanced, attributing to the CT effect from fluorene donor to NFSO acceptor unit. The PL spectrum of polymers in film exhibited weak redshift and broadening with increased NFSO unit. The maximum emission peak red shifted from 437 nm for PNFSO2 to 447 nm for PNFSO10, and the full width at half maximum (FWHM) changed from 45 nm for PNFSO2 to about 66 nm for PNFSO10. The optical band gap ($E_{\mathrm{g}}^{\mathrm{opt}}$) was calculated from the UV–vis absorption band edge in film by the equation $E_{\mathrm{g}}^{\mathrm{opt}} = 1240/\lambda_{\mathrm{edge}}$. Hence, the $E_{\mathrm{g}}^{\mathrm{opt}}$ were 2.92, 2.91, and 2.90 eV for polymer PNFSO2, PNFSO5, and PNFSO10, respectively. The detailed photophysical parameters are summarized in Table 2.

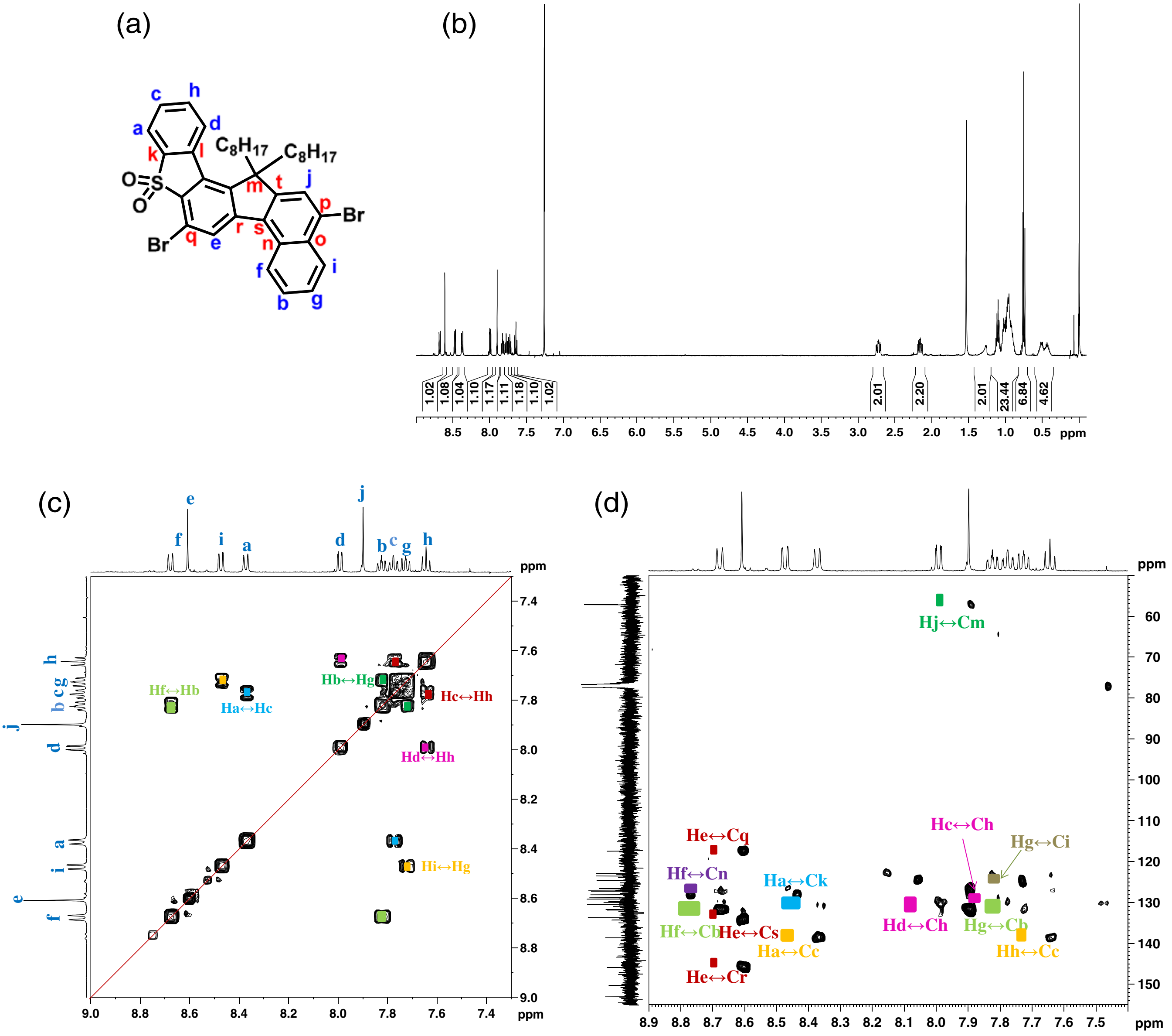

FIGURE 1 Molecular structure of monomer (a), ^{1}H NMR spectrum (b), ^{1}H-^{1}H COSY spectrum (c), and ^{1}H-^{13}C HMBC spectrum (d). [Color figure can be viewed at wileyonlinelibrary.com]

TABLE 1 Molecular Weight and Thermal Properties of Polymers

Polymer	M_n (kDa)	PDI	T_m (°C)	T_d^{a} (°C)	E_{ox} (V)	E_{red} (V)	HOMO (eV)	LUMO (eV)	$E_g^{opt,b}$ (eV)
PFO	25.8	2.26	148	424	1.34	−2.25	−5.75	−2.16	2.93
PNFSO2	35.8	2.34	132	423	1.35	−2.22	−5.76	−2.19	2.92
PNFSO5	34.7	1.93	135	420	1.36	−2.16	−5.77	−2.25	2.91
PNFSO10	42.8	1.91	139	424	1.36	−2.15	−5.77	−2.26	2.90

[a] Corresponding to 5 wt % weight loss.

[b] Calculated from the UV–vis absorption band edge of the molecule film by the equation, $E_g^{\text{opt}} = 1240/\lambda_{\text{edge}}$.

To evaluate the effect of NFSO unit on optical properties of polymer, we also made a contrastive study about the UV–vis absorption and PL properties for polymer PNFSO5 and PFSO5. The PL spectra of PNFSO5 exhibited significant blue-shift in toluene and as film state compared with that for PFSO5, which determined by the weak CT effect attributed to the SO unit in side chain for PNFSO5 (Supporting Information Fig. S2). Figure 5 showed the UV–vis absorption and PL spectra of the

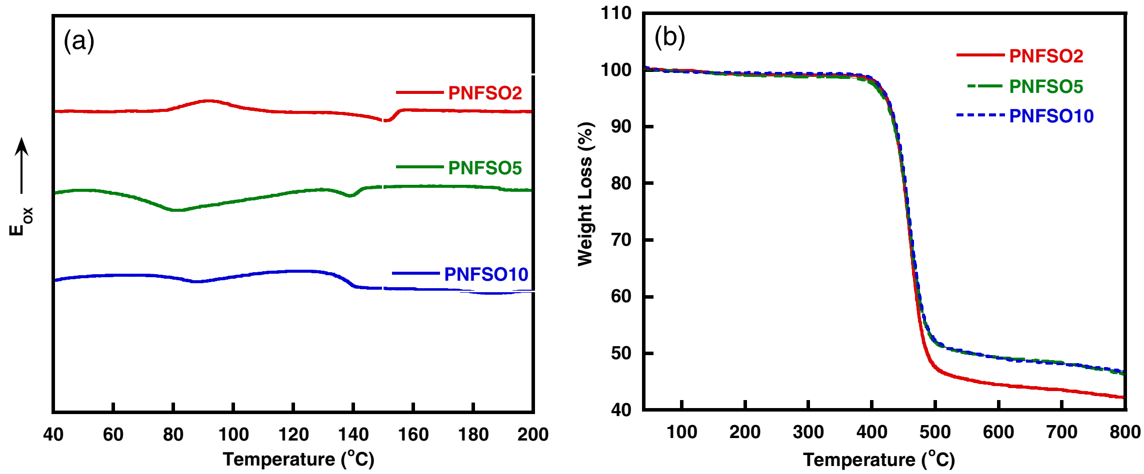

FIGURE 2 DSC and TGA curves of polymers. [Color figure can be viewed at wileyonlinelibrary.com]

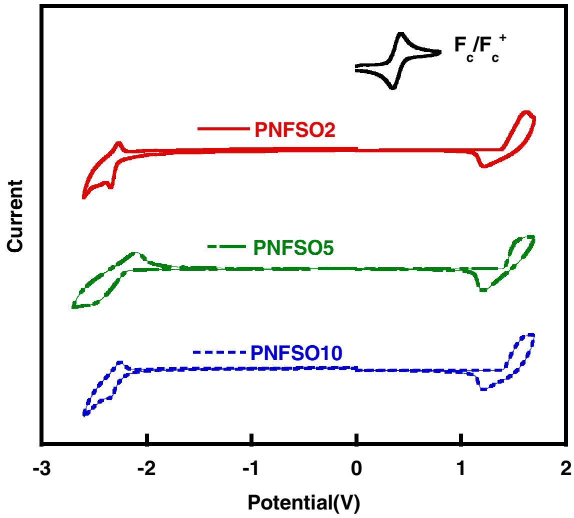

FIGURE 3 Cyclic voltammetry characteristics of polymers. [Color figure can be viewed at wileyonlinelibrary.com]

PNFSO5 and PFSO5 in different polar solution. The absorption spectra of polymers in solution with different polarity are almost identical; however, the PL spectra gradually became broadened from toluene, THF to $CHCl_3$ solution and bathochromic shift by about 26 nm for PFSO5. On the contrary, the main peak close to 416 nm was almost unchanged, and the shoulder peak was red-shifted from 437 to 442 nm for PNFSO5, respectively, indicating that the CT character of the polymers in the excited state and the stronger CT effect for PFSO5. In same solution, the stokes shifts of PNFSO5 was smaller than that of PFSO5, which can be illustrated that the asymmetric structure from NFSO unit may induce a twisted polymeric backbone, and the SO unit in the side chain could weaken CT effect. The photoluminescence quantum efficiencies (Q_{PL}) of the polymers are in the range of 46%–51%, which are higher than that of PFO homopolymer (Table 2).

DFT Calculation

To understand the frontier molecular orbitals and molecular backbone conformation of the polymers, DFT calculations

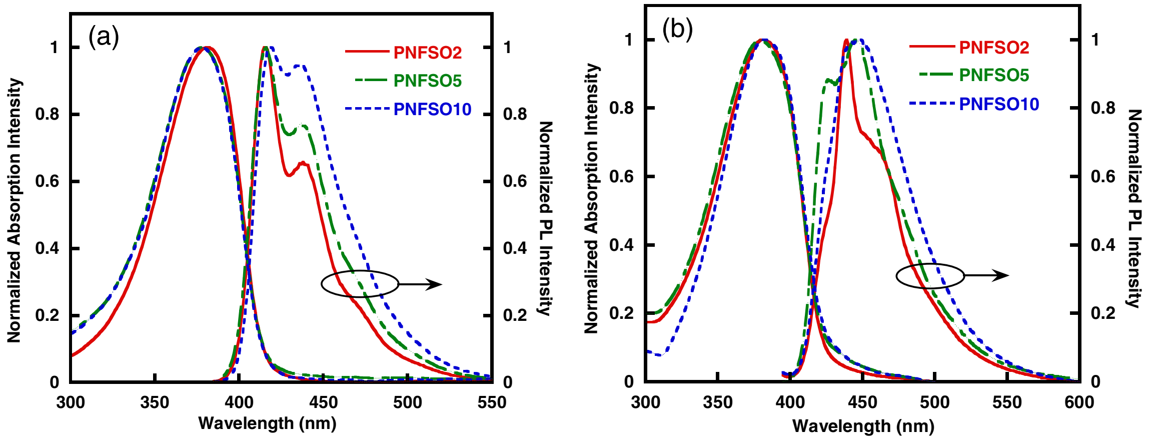

FIGURE 4 UV–vis absorption and PL spectra of polymers in toluene solution with concentration of 1 × 10^{-5} g mL^{-1} (a) and solid film (b). [Color figure can be viewed at wileyonlinelibrary.com]

TABLE 2 Photophysical Properties of Polymers

	λ_{max}^{UV} (nm)					λ_{max}^{PL} (nm)			Q_{PL}
Polymer	Toluene	$CHCl_3$	Film	λ_{onset} (nm)	$E_g^{opt,a}$ (eV)	Toluene	$CHCl_3$	Film	(%)
PFO	380	376	377	424	2.93	416, 438	416	440	32
PNFSO2	381	371	382	424	2.92	416, 437	417	439	46
PNFSO5	378	376	379	426	2.91	416, 436	418	445	58
PNFSO10	378	377	381	428	2.90	419, 436	443	449	51

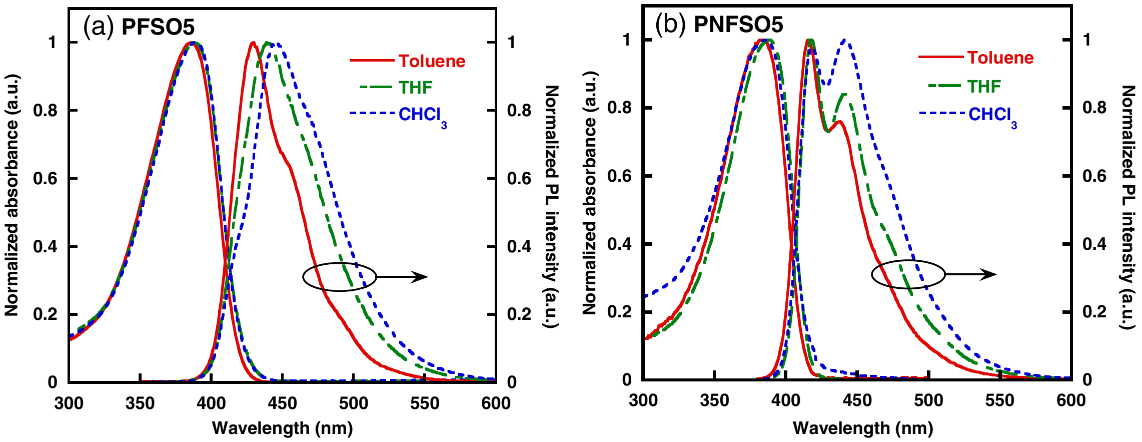

FIGURE 5 The UV–Vis absorption spectra and PL spectra in solution for PFSO5 (a) and PNFSO5 (b). [Color figure can be viewed at wileyonlinelibrary.com]

were performed by using the B3LYP/6-31G(d) in the Gaussian 09.[34] All alkyl chains were replaced by methyl groups and pentamers were used as the main chromophores of each polymer to simplify the calculation. Model molecules of polymers PFO (FFFFF), PNFSO (FF-NSO-FF) were constructed, respectively. Figure 6 depicted the calculated molecular conformations and frontier molecular orbitals of the model molecules. The molecular conformation of FF-NSO-FF showed clear distortion attributed to the asymmetric linked NFSO moiety in pentamers, then that of FFFFF exhibited linear typed

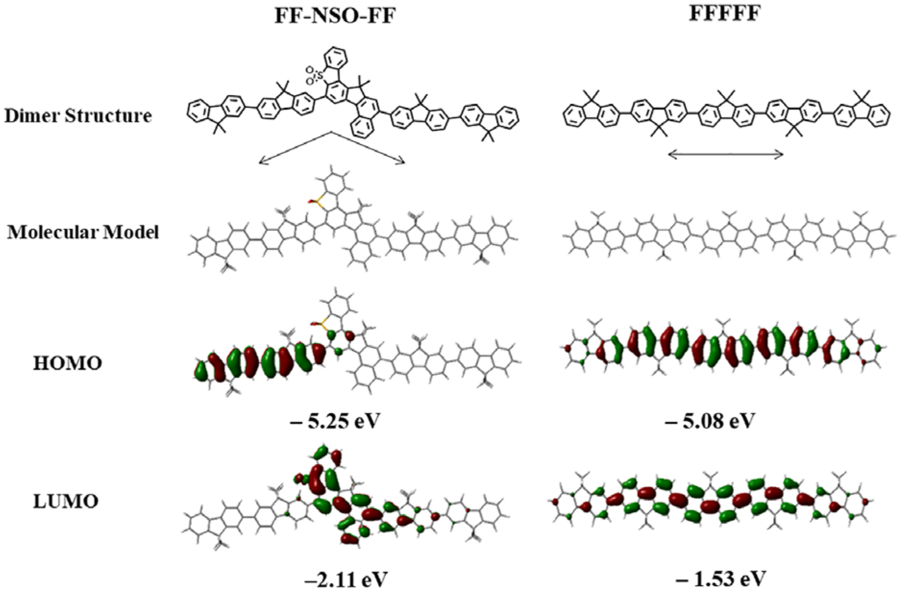

FIGURE 6 Structure and spatial distribution of the HOMO and LUMO in model molecules. [Color figure can be viewed at wileyonlinelibrary.com]

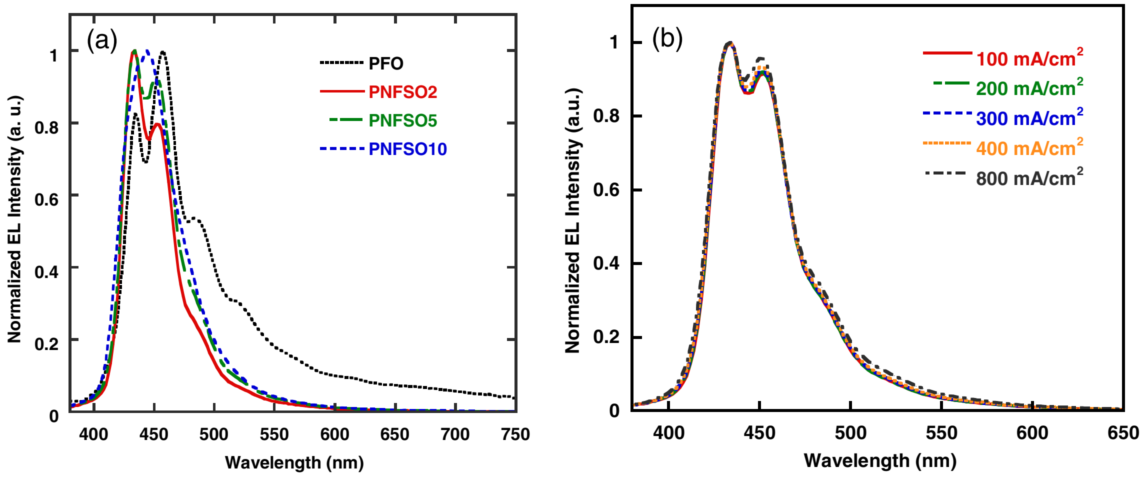

FIGURE 7 EL spectra for all polymers (a) and EL spectra with the variation of current densities for PNFSO5 (b). [Color figure can be viewed at wileyonlinelibrary.com]

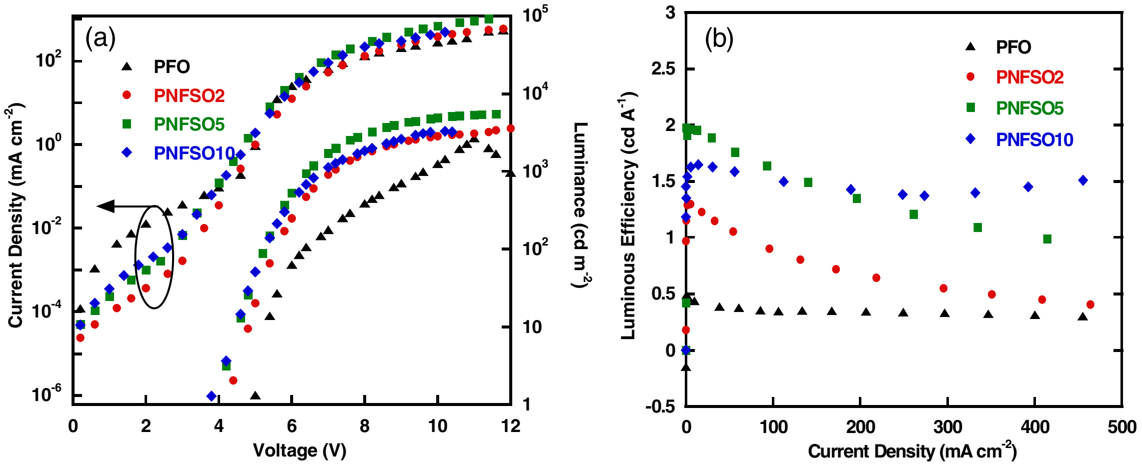

FIGURE 8 *J-V-L* curves (a) and LE-*J* curves (b) of devices based on polymers. [Color figure can be viewed at wileyonlinelibrary.com]

conformation. The HOMO and LUMO were delocalized over the pentamer (FFFFF), whereas, the molecular orbital distribution of FF-NSO-FF was different from that of the former completely. The HOMO was mainly localized at fluorene moiety, while its LUMO was mainly distributed on the electron deficient NFSO unit.[35] Such electron distribution endows the FF-NSO-FF inherent intramolecular CT property. The calculated $E_{\mathrm{HOMO}}/E_{\mathrm{LUMO}}$ of FF-NSO-FF was −5.25/−2.11 eV, which was deeper than −5.08/−1.53 eV of FFFFF, displaying good agreement with the experimental results measured by the CV.

EL Properties

To evaluate the EL properties of polymers, a single-layer device with the structure of ITO/PEDOT:PSS/EML(60 nm)/Ba/Al was fabricated. The EL spectra of polymers were presented in Figure 7(a). The twisted backbone structure of copolymers can disrupt the extended π-conjugation, so the EL profiles of copolymers were in deep-blue emission and blue-shifted slightly compared to PFO. While increasing the amount of NFSO unit, the emission peak goes from 432 nm for PNFSO2 upward to 442 nm for PNFSO10 arising from weak CT effect. The EL spectra of PNFSO5 under increased current densities from 100 to 800 mA cm^{-2} was shown in Figure 7 (b). It was suggested that PNFSOs exhibited current-density-independent EL spectra, implying the excellent stability of the resulting polymers.

Figure 8 illustrated the current density (*J*) and luminance (*L*) as functions of driving voltage (*V*) (*J-V-L*) characteristics and the luminous efficiencies-current densities (LE-*J*) curves of devices. It can be seen that the leakage current density in PFO device is higher than that in other device, which can be attributed to a larger electron injection barrier at the cathode/emissive layer interface for PFO device from E_{LUMO} of Table 1 and the unbalanced hole and electron fluxes of PFO device in Figure 9. With the increase of NFSO moiety in polymer, the turn-on voltage gradually decreased, and luminance and current density enhanced evidently at same turn-on voltage [Fig. 8(a)]. Seen from Figure 8(b), in comparison with homopolymer PFO, the LE of the copolymers were improved

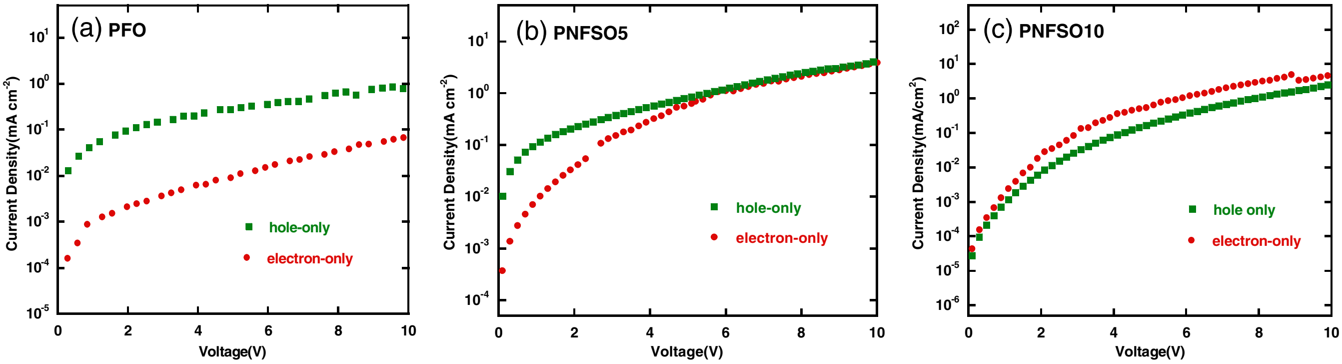

FIGURE 9 *J-V* characteristics of the hole-/electron-only devices of PFO (a), PNFSO5 (b) PNFSO10 (c). [Color figure can be viewed at wileyonlinelibrary.com]

TABLE 3 Device Performances of Polymers

Polymer	V_{on}[a] (V)	LE_{max} (cd A^{-1})	L_{max} (cd m^{-2})	CIE[b] (*x*,*y*)
PFO	4.6	0.49	2691	(0.18,0.18)
PNFSO2	4.3	1.30	3573	(0.16,0.06)
PNFSO5	4.0	1.96	5481	(0.16,0.07)
PNFSO10	4.0	1.65	3279	(0.16,0.08)

[a] Corresponding to 1 cd m^{-2}.

[b] Measured at 36 mA cm^{-2}.

conspicuously, and we can note that all devices showed relatively low roll-off of luminous efficiency with the increasing of current densities, which was favorable for the long-term working stabilities of the devices.

The device performance data were summarized in Table 3. It can be seen that the PFO exhibited low device efficiency with LE_{max} of 0.49 cd A^{-1} and CIE coordinates of (0.18, 0.18). However, the PF-FSO5 exhibited better EL performance with LE_{max} of 0.77 cd A^{-1} and CIE coordinates of (0.17, 0.13).[25] In contrary, the combination property of the copolymers PNFSOs have a dramatically enhancement with respect to PFO and PF-FSO5. With varying content of NFSO unit, the EL profiles showed deep blue light emission, and all copolymers achieved

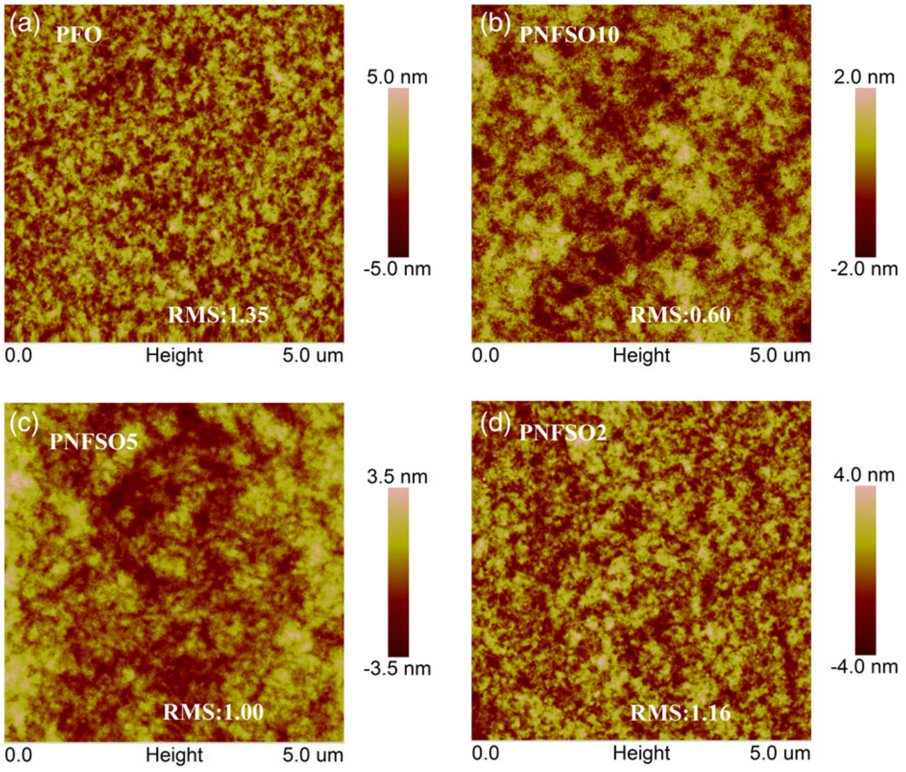

FIGURE 10 AFM images of all polymers. [Color figure can be viewed at wileyonlinelibrary.com]

superior CIE coordinate with $CIE_x + CIE_y < 0.3$ and $CIE_y < 0.10$, which was benefited from the twisted-structure NFSO unit. The best device performances were achieved based on PNFSO5, which exhibited the maximum luminous efficiencies (LE_{max}) of 1.96 cd A^{-1} and the maximum luminance (L_{max}) of 5481 cd m^{-2}, associated with the characteristic deep blue emission with CIE coordinates of (0.16, 0.07). The improved performance can be attributed to a lower leakage current (Fig. 8), the balanced hole and electron fluxes (Fig. 9), and improved PLQY (Table 2).

To explore the efficiency improvement of PNFSOs, the single charge carrier devices were fabricated and their current density-voltage characteristics (*J-V*) are shown in Figure 9. The hole-only device of PFO exhibited much higher current densities than the corresponding electron-only device in the entire applied voltage range of 0–10 V. The introducing of electron-withdrawing NFSO unit into polymer enhanced electron affinity, and thus, increased electron current and bring about more balanced electron and hole transport and further improved device performance of PNFSO5. Furthermore, the electron fluxes exceed the hole fluxes in PNFSO10, which also explains why the device performance decreased when the NFSO moiety content further increased from 5% to 10%.

Film Morphology

The direct surface topographies of polymers were investigated by AFM and the relevant images were shown in Figure 10. The root-mean-square (RMS) roughness value recorded for PFO was 1.35 nm, and the RMS value gradually reduced after introducing NFSO unit into PFO backbone from 1.16 nm for PNFSO2 to 0.60 nm for PNFSO10, which demonstrated that the polymers containing the NFSO moiety have an excellent film forming ability. There was an inverse correlation between the content of NFSO unit and the RMS values. The more proportion of NFSO unit accelerated the more distorted structure of polymer to reduce the π-π stacking of polymer chains, which made it difficult for them to aggregate in film state, and thereby enhance the film forming ability.

CONCLUSIONS

In summary, a novel polycyclic aromatic compound 2,8-dibromo-14,14-dioctyl-14*H*-benzo[*b*]benzo[5,6]fluoreno [1,2-*d*] thiophene 9,9-dioxide was designed and synthesized, and was incorporated into PFO backbone. The resulting polymers exhibited good thermal stability with thermal decomposition temperature over 420 °C and higher luminescent efficiency with PLQY over 45%. Compared with poly(9,9-dialkylfluorene-2,7-diyl)s (PFO), the LUMO energy levels of the copolymer PNFSOs slightly decreased with the increase of NFSO content in copolymer backbone from −2.16 eV for PFO to −2.26 eV for PNFSO10. The PL spectra of copolymers blue-shifted to acquire deep blue emission due to the suitable twisted structure. The copolymers show stable EL spectra with the increase of current densities in the range of 100–800 mA cm^{-2}. The champion performance was achieved from the device based on PNFSO5, which showed a low turn-on voltage of 4.0 V, a maximum luminous efficiency of 1.96 cd A^{-1}, with CIE coordinates of (0.16, 0.07), respectively. The result indicated that our designed strategy effectively weakened CT effect compared with PFSO5 and improved the EL efficiency and achieved deep-blue light emission with respect to PF-FSO5, indicating that the twisted-structure NFSO unit had a great potential for adjusting the polymers blue-light emission and enhancement of EL efficiency.

ACKNOWLEDGMENTS

The authors are grateful for the financial support from the National Key Research and Development Program of China(No. 2016YFB0401302) funded by MOST, the Science and Technology Program of Guangdong Province, China (No. 2017A050503002), the National Natural Science Foundation of China (No. 21704027), and the Natural Science Foundation of Jiangsu Province (Grant No. BK20141151).

REFERENCES AND NOTES

1 L. Ying, C. L. Ho, H. B. Wu, Y. Cao, W. Y. Wong, *Adv. Mater.* **2014**, *26*, 2459.

2 M. S. AlSalhi, J. Alam, L. A. Dass, M. Raja, *Int. J. Mol. Sci.* **2011**, *12*, 2036.

3 R. P. Xu, Y. Q. Li, J. X. Tang, *J. Mater. Chem. C* **2016**, *4*, 9116.

4 S. Reineke, F. Lindner, G. Schwartz, N. Seidler, K. Walzer, B. Lussem, K. Leo, *Nature* **2009**, *459*, 234.

5 T. Guo, W. K. Zhong, J. H. Zou, L. Ying, W. Yang, J. B. Peng, *Acta Polym. Sin.* **2016**, *3*, 360.

6 T. Guo, L. Yu, B. F. Zhao, Y. H. Li, Y. Tao, W. Yang, Q. Hou, H. B. Wu, Y. Cao, *Macromol. Chem. Phys.* **2012**, *213*, 820.

7 L. Yu, J. Liu, S. J. Hu, R. F. He, W. Yang, H. B. Wu, J. B. Peng, R. D. Xia, D. D. C. Bradley, *Adv. Funct. Mater.* **2013**, *23*, 4366.

8 K. M. Schelkle, M. Bender, K. Jeltsch, T. Buckup, K. Mullen, M. Hamburger, U. H. F. Bunz, *Angew. Chem. Int. Ed.* **2015**, *54*, 14545.

9 K. H. Weinfurtner, H. Fujikawa, S. Tokito, Y. Taga, *Appl. Phys. Lett.* **2000**, *76*, 2502.

10 E. J. W. List, R. Guentner, P. S. de Freitas, U. Scherf, *Adv. Mater.* **2002**, *14*, 374.

11 K. Becker, J. M. Lupton, J. Feldmann, B. S. Nehls, F. Galbrecht, D. Q. Gao, U. Scherf, *Adv. Funct. Mater.* **2006**, *16*, 364.

12 L. P. Lu, D. Kabra, K. Johnson, R. H. Friend, *Adv. Funct. Mater.* **2012**, *22*, 144.

13 F. Lemasson, N. Berton, J. Tittmann, F. Hennrich, M. M. Kappes, M. Mayor, *Macromolecules* **2012**, *45*, 713.

14 J. H. Cook, J. Santos, H. Y. Li, H. A. Al-Attar, M. R. Bryce, A. P. Monkman, *J. Mater. Chem. C* **2014**, *2*, 5587.

15 J. H. Cook, J. Santos, H. A. Al-Attar, M. R. Bryce, A. P. Monkman, *J. Mater. Chem. C* **2015**, *3*, 9664.

16 X. C. Wang, L. Zhao, S. Y. Shao, J. Q. Ding, L. X. Wang, X. B. Jing, F. S. Wang, *Macromolecules* **2014**, *47*, 2907.

17 S. M. King, S. I. Hintschich, D. Dai, C. Rothe, A. P. Monkman, *J. Phys. Chem. C* **2007**, *111*, 18759.

18 X. C. Wang, L. Zhao, S. Y. Shao, J. Q. Ding, L. X. Wang, X. B. Jing, F. S. Wang, *Polym. Chem.* **2014**, *5*, 6444.

19 W. Xue, J. Y. Lin, B. Liu, N. E. Shi, M. N. Yu, W. D. Wu, W. S. Zhu, L. H. Xie, L. H. Wang, W. Huang, *Polymer* **2018**, *153*, 338.

20 M. S. Liu, X. Jiang, S. Liu, P. Herguth, A. K.-Y. Jen, *Macromolecules* **2002**, *35*, 3532.

21 Y. Yang, L. Yu, Y. Xue, Q. H. Zou, B. Zhang, L. Ying, W. Yang, J. B. Peng, Y. Cao, *Polymer* **2014**, *57*, 1698.

22 A. W. Grice, A. Tajbakhsh, P. L. Burn, D. D. C. Bradley, *Adv. Mater.* **1997**, *9*, 1174.

23 Y. Y. Li, H. B. Wu, J. H. Zou, L. Ying, W. Yang, Y. Cao, *Org. Electron.* **2009**, *10*, 901.

24 L. W. Hu, Y. Yang, J. Xu, J. F. Liang, T. Guo, B. Zhang, W. Yang, Y. Cao, *J. Mater. Chem. C* **2016**, *4*, 1305.

25 Y. W. Fang, J. Liu, Y. H. Zhang, T. Guo, F. Huang, W. Yang, Y. Cao, *Sci. China Chem.* **2017**, *60*, 1356.

26 J. Xu, Y. Yang, L. W. Hu, T. Guo, B. Zhang, W. Yang, *Dyes Pigm.* **2017**, *138*, 245.

27 S. Zhao, J. F. Liang, T. Guo, Y. Wang, X. Chen, D. H. Fu, J. B. Xiong, L. Ying, W. Yang, J. B. Peng, Y. Cao, *Org. Electron.* **2016**, *38*, 130.

28 M. Ranger, D. Rondeau, M. Leclerc, *Macromolecules* **1997**, *30*, 7686.

29 X. Wang, Z. M. Zhong, S. Zhao, T. Guo, J. X. Jiang, J. H. Zou, L. Ying, J. B. Peng, Y. Cao, *Org. Electron.* **2018**, *55*, 157.

30 T. Guo, L. Yu, B. F. Zhao, L. Ying, H. B. Wu, W. Yang, Y. Cao, *J. Polym. Sci., Part A: Polym. Chem* **2015**, *53*, 1043.

31 J. L. Bredas, R. Silbey, D. S. Boudreaux, R. R. Chance, *J. Am. Chem. Soc.* **1983**, *105*, 6555.

32 E. Oguzhan, H. Bilgili, F. B. Koyuncu, E. Ozdemir, S. Koyuncu, *Polymer* **2013**, *54*, 6283.

33 J. F. Liang, J. Cui, T. Guo, F. Peng, Y. C. Li, L. Ying, W. Yang, J. B. Peng, Y. Cao, *Org. Electron.* **2017**, *51*, 111.

34 M. J. Frisch, G. W. Trucks, H. B. Schlegel, G. E. Scuseria, M. A. Robb, J. R. Cheeseman, G. Scalmani, V. Barone, B. Mennucci, G. A. Petersson, H. Nakatsuji, M. Caricato, X. Li, H. P. Hratchian, A. F. Izmaylov, J. Bloino, G. Zheng, J. L. Sonnenberg, M. Hada, M. Ehara, K. Toyota, R. Fukuda, J. Hasegawa, M. Ishida, T. Nakajima, Y. Honda, O. Kitao, H. Nakai, T. Vreven, J. A. Montgomery Jr. , J. E. Peralta, F. Ogliaro, M. Bearpark, J. J. Heyd, E. Brothers, K. N. Kudin, V. N. Staroverov, R. Kobayashi, J. Normand, K. Raghavachari, A. Rendell, J. C. Burant, S. S. Iyengar, J. Tomasi, M. Cossi, N. Rega, J. M. Millam, M. Klene, J. E. Knox, J. B. Cross, V. Bakken, C. Adamo, J. Jaramillo, R. Gomperts, R. E. Stratmann, O. Yazyev, A. J. Austin, R. Cammi, C. Pomelli, J. W. Ochterski, R. L. Martin, K. Morokuma, V. G. Zakrzewski, G. A. Voth, P. Salvador, J. J. Dannenberg, S. Dapprich, A. D. Daniels, O. Farkas, J. B. Foresman, J. V. Ortiz, J. Cioslowski, D. J. Fox, *Gaussian 09, Revision A. 02*; Gaussian, Inc.: Wallingford, CT, **2009**.

35 I. I. Perepichka, I. F. Perepichka, M. R. Bryce, L. O. Pålsson, *Chem. Commun.* **2005**, *27*, 3397.